Applied Catalysis B: Environmental 189 (2016) 226–232

Contents lists available at ScienceDirect

Applied Catalysis B: Environmental

journal homepage: www.elsevier.com/locate/apcatb

Facile synthesis of hierarchical Cu_2O nanocubes as visible light photocatalysts

Santosh Kumar[a], Christopher M.A. Parlett[a], Mark A. Isaacs[a], Danielle V. Jowett[b], Richard E. Douthwaite[b], Martin C.R. Cockett[b], Adam F. Lee[a,*]

[a] European Bioenergy Research Institute, Aston University, Birmingham B4 7ET, UK
[b] Department of Chemistry, University of York, York YO10 5DD, UK

ARTICLE INFO

Article history:
Received 9 December 2015
Received in revised form 10 February 2016
Accepted 16 February 2016
Available online 20 February 2016

Keywords:
Photocatalysis
Copper oxide
Nanomaterials
Hierarchical
Hydrogen

ABSTRACT

Hierarchically structured Cu_2O nanocubes have been synthesized by a facile and cost-effective one-pot, solution phase process. Self-assembly of 5 nm Cu_2O nanocrystallites induced through reduction by glucose affords a mesoporous 375 nm cubic architecture with superior visible light photocatalytic performance in both methylene blue dye degradation and hydrogen production from water than conventional non-porous analogues. Hierarchical nanocubes offer improved accessible surface active sites and optical/electronic properties, which act in concert to confer 200–300% rate-enhancements for the photocatalytic decomposition of organic pollutants and solar fuels.

1. Introduction

Semiconductor metal oxides have attracted great interest as photocatalytic materials for wide-ranging technological applications including wastewater remediation [1], solar fuels via both H_2 production [2] and CO_2 reduction [3], and microbial disinfection [4–6]. Historically, there has been extensive academic and commercial interest in titania photocatalysts. However the past decade has seen a dramatic surge of interest in alternative oxide and associated composite catalyst systems. Amongst these, copper oxide has featured prominently as an earth abundant and low cost, narrow band-gap (2–2.22 eV) p-type intrinsic semiconductor [7]. In addition to its suitability for visible light excitation, the conduction and valence band energies of Cu_2O render it a promising photocatalyst for water splitting and CO_2 reduction [8]. The photostability of Cu_2O in aqueous media remains a challenge [9] due to its low reduction potential which lies within the band gap. However this undesirable photocorrosion in water is a strong function of oxide morphology/facet termination [10]. A variety of Cu_2O nanocrystal morphologies and sizes have been synthesised to date, including wires, flowers, octahedra, dodecahedra, cubes and spheres, all of which exhibit good visible light photoactivity for the aqueous phase degradation of organic dyes which serve as models of waste water pollutants [9,11–15].

Functional hierarchical nanostructures (in which superstructures are created through assemblies of smaller units) have also attracted significant recent interest due to their often superior (and tunable) electronic, optical and catalytic properties [16–20]. Hierarchical photocatalysts represent a particularly exciting development, wherein the hierarchy may permit control of mass transport [21], light absorption [22] and heterojunction interfaces in nanocomposites. Hence, it is of interest to explore whether hierarchical Cu_2O nanostructures also exhibit enhanced photocatalytic properties; pure hierarchical cuprous oxide [18,23] and nanocomposites thereof with e.g. Cu [24] or ZnO [25], have shown promise in the decomposition of model organic waste water pollutants and in solar fuels production.

Herein, we demonstrate the first facile one-pot and low temperature chemical route to the synthesis of hierarchical 375 nm Cu_2O nanocubes comprised of 5 nm sub-units, which exhibit superior visible light photocatalytic performance for methylene blue (MB) decomposition and H_2 production from water.

* Corresponding author.
E-mail address: a.f.lee@aston.ac.uk (A.F. Lee).

http://dx.doi.org/10.1016/j.apcatb.2016.02.038

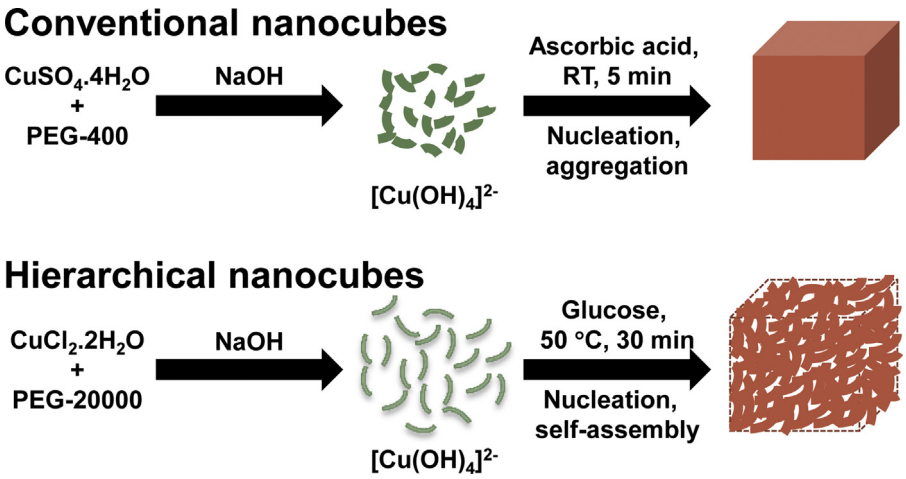

Scheme 1. Synthetic routes to conventional and hierarchical Cu_2O nanocubes.

2. Experimental

2.1. Nanocube synthesis

$CuCl_2{\cdot}2H_2O$ (ACROS Organics, 99.0%), $CuSO_4{\cdot}5H_2O$ (Sigma 99.0%), Glucose (Sigma), Poly (ethylene glycol) (PEG, average M_n 20,000, Sigma), Poly (ethylene glycol) (PEG, average M_n 400, Sigma), Ascorbic acid (Sigma, 99.9%), NaOH pellets, (Fisher Chemicals), and MB (Sigma, 95.0%) were used as received. All other chemical reagents used in this work were analytically pure and used without further purification.

Conventional Cu_2O nanocubes were prepared following previous literature reports [26]. In a typical procedure, 0.01 M $CuSO_4{\cdot}5H_2O$ solution (8 ml) was mixed with 32 ml of 0.031 M PEG-400 and stirred for 5 min at room temperature. To this solution, 0.15 M NaOH (ml) was added followed by 0.0.02 M ascorbic acid (10 ml) drop wise and stirred for 5 min at room temperature. Further the solution was kept undisturbed for 30 min. The resulting precipitate was washed several times with ethanol and dried in vacuum oven at 40 °C for 12 h.

Hierarchical Cu_2O nanocubes were prepared by a facile and one pot chemical process. Typically 200 mg PEG-20000 and 200 mg $CuCl_2.2H_2O$ were dissolved in 100 ml of H_2O separately and stirred for 15 min to ensure that the PEG and $CuCl_2$ dissolved completely. The PEG solution was added to $CuCl_2$ solution with stirring for 15 min. To this mixture, 3 ml of 3 M NaOH was added, under constant stirring. A blue color solution of $[Cu(OH)_4]^{2-}$ was soon produced. After stirring for 15 min, 0.27 g of glucose was added at 50 °C, with constant stirring for 30 min. The blue color gradually turned into a red color. The red color precipitate was centrifuged, washed several times with distilled water, and dried in a vacuum oven at 40 °C for 12 h.

Platinum promoted nanocubes were prepared for water splitting via a photoreduction method. In brief, 25 mg of Cu_2O nanocubes and an appropriate amount of aqueous H_2PtCl_6 solution (1 mg ml^{-1}) were dispersed in 20 ml of a 20 vol% aqueous methanolic solution (as a hole scavenger), and then irradiated under a 200 W Hg-Xe light source for 2 h at room temperature. Pt loaded Cu_2O nanocubes were separated subsequently by centrifugation at 5000 rpm and drying at 60 °C for 4 h in a vacuum oven.

Powder X-ray diffraction (XRD) pattern was recorded on a Bruker-AXS D8 ADVANCE diffractometer operated at 40 kV voltages and 40 mA current using Cu Kα radiation in the range 10–80°. Surface analysis for the as-prepared products was performed by X-ray photoelectron spectroscopy using a Kratos Axis HSi spectrometer and monochromated Al Kα X-ray source operated at 90 W. Binding energies were referenced relative to adventitious carbon at 284.6 eV. Spectral processing was performed using CasaXPS version 2.3.16. Catalyst morphology was investigated by field-emission SEM using a JEOL (JSM-7000F) microscope operating at an accelerating voltage of 20 kV. TEM analysis was performed on a JEOL JEM-2100 transmission electron microscope operating at an accelerating voltage of 200 kV. Nitrogen adsorption measurements were performed with a Quantachrome NOVA 4000e porosimeter. Brunauer–Emmett–Teller (BET) surface areas were calculated over the relative pressure range 0.01–0.2. Pore size distributions were calculated by applying the BJH method to the desorption isotherm for relative pressures >0.35. UV–vis spectra were measured on a Thermo Scientific Evo220 spectrometer. Photoluminescence spectra of the as-prepared samples were recorded on a F-4500FL spectrometer at an excitation wavelength of 560 nm.

2.2. Methylene blue photodegradation

Photocatalytic testing of the Cu_2O samples for the degradation of the MB dye were carried out at room temperature in a sealed 120 ml quartz photoreactor. Test solutions were prepared by mixing 50 ml of MB solution (10 ppm) and 25 mg of either hierarchical or conventionally prepared Cu_2O nanocubes to form an aqueous dispersion. Prior to irradiation, the test solution was kept in the dark for 60 min under constant stirring to establish the adsorption-desorption equilibrium. Subsequently, the reaction mixture was irradiated by a 200 W Oriel Instruments 66002 Hg-Xe arc lamp employing a 420 nm cut-off filter to remove UV radiation, under stirring. Aliquots of the reaction mixture were periodically withdrawn and centrifuged to separate the catalyst, and UV–vis absorption spectra recorded on the filtrate to monitor the extent of MB reaction.

2.3. Hydrogen evolution

Photocatalytic H_2 production was performed over platinized Cu_2O samples in a sealed 120 ml quartz photoreactor at room temperature using a 200 W Hg-Xe arc lamp whose spectral output is shown in Fig. S1. 25 mg of Cu_2O samples was added to 20 ml of 0.5 M Na_2SO_3 aqueous solution (sulfite as a hole scavenger), and the suspension subsequently ultrasonicated for 5 min to obtain a uniform dispersion. Before each experiment, the reaction mixture was purged with He for 1 h to degas the solution and remove air from the system. H_2 evolution was measured by gas chromatography (Shimadzu Tracera GC-2010 Plus) with He as a carrier gas and a Barrier Ionization Detector.

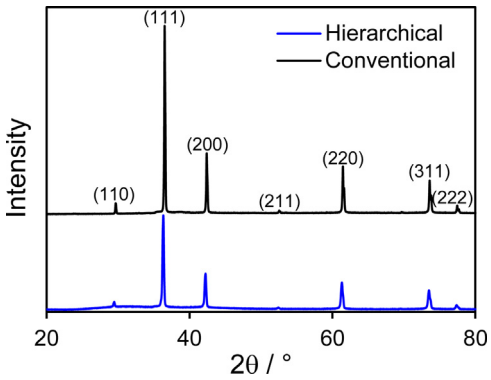

Fig. 1. Powder XRD patterns of conventional and hierarchical Cu_2O nanocubes. Diffractograms offset for clarity.

3. Results and discussion

Hierarchical and conventional Cu_2O nanocubes, comprising self-assembled nanoparticle aggregates, were synthesised from different copper (II) precursors employing long and short PEG chains respectively as structure-directing agents (Scheme 1). In this one-pot process, electrostatic interactions between Cu^{2+} ions and the hydroxyl groups in the PEG control the distribution of Cu_2O nuclei formed throughout the polymer matrix during the reduction step induced by either glucose (hierarchical) or ascorbic acid (conventional) in the presence of NaOH as a precipitant [23]. This distribution in turn regulates the nanoparticle morphology, and their aggregation into the final superstructure to minimize the total system energy.

The crystallographic structure and phase purity of the nanocubes was first investigated by powder XRD (Fig. 1), which confirmed the exclusive presence of crystalline cubic Cu_2O (JCPDS#73-0687) in both cases, with characteristic reflections at 29.7°, 36.6°, 42.5°, 52.5°, 61.6°, 73.7° and 77.5° ascribed to the (1 1 0), (1 1 1), (2 0 0), (2 1 1), (2 2 0), (3 1 1) and (2 2 2) planes of cuprous oxide respectively.

Field-emission scanning electron microscopy (FESEM) and transmission electron microscopy (TEM) were subsequently employed to determine the morphology and size of the resultant Cu_2O nanostructures (Fig. 2). FESEM revealed that both synthetic routes in Scheme 1 yielded uniform nanocubes with mean side lengths around 375 nm. However, higher resolution imaging (Fig. 2**a** and **c** inset) showed significant differences in the surface texture of each nanocube type: those prepared by conventional synthesis using the sulfate precursor/ascorbic acid reductant exhibit very smooth facets with clearly defined edges and vertices; in contrast the new synthesis affords rough surfaces constructed from tightly-packed aggregates of individual Cu_2O particles with dimensions <20 nm. Dark field TEM (Fig. 2b and d) highlights these textural differences, with conventional nanocubes appearing extremely smooth and regular, whereas the hierarchical nanocubes have poorly defined edges and vertices consistent with the FESEM images. The volume-averaged Cu_2O crystallite size for the hierarchical nanocubes determined by XRD of around 20 nm was significantly larger than that derived by TEM. This difference may reflect the presence of an inner core within the hierarchical nanocubes which dominates the X-ray diffractogram, and/or the localised nature of high-resolution electron microscopy and concomitant superior ability to discriminate individual Cu_2O nanocrystals present within a larger agglomerate.

High resolution transmission electron microscopy (HRTEM) of the hierarchical nanocubes shown in Fig. 3 confirms that they are indeed aggregates of many smaller nanocrystallites with mean diameters of approximately 5 nm. The interplanar lattice spacings of these nanocrystals of 0.242 nm (Fig. 3d) corresponds to the (111) plane of cubic Cu_2O in accordance with XRD phase identification.

Corresponding DRUVS absorption spectra (Fig. 4a) exhibited a similar band edge for the conventional and hierarchical Cu_2O nanocubes of ca. 640 nm. The associated band gap was calculated using the following Eq. (1):[27]

$$\alpha h\nu = A\left(h\nu - E_g\right)^{\eta} \quad (1)$$

where α, h, ν, Eg and A are the absorption coefficient, Planck's constant, light frequency, band gap energy, and a proportionality constant respectively. The variable η depends on the nature of the optical transition during photon absorption. For direct band gap materials such as Cu_2O, Eg can be estimated from a Tauc plot of $(\alpha h\nu)$ [2] versus $h\nu$ wherein $\eta = 0.5$, with the optical absorption coefficient obtained from the Kubelka–Munk function, giving E_g's of 2.00 and 2.05 eV respectively for conventional and hierarchical Cu_2O nanocubes (Fig. 4b). The small blue shift for the hierarchical Cu_2O nanocubes may reflect quantum size effects due to its smaller constituent particles [28].

Valence band maximum (VBM) edge potentials for conventional and hierarchical Cu_2O nanocubes were determined by valence band XPS (Fig. 5a) from the intercept of the tangent to the density of states at the Fermi edge as 0.57 eV and 0.55 eV, respectively, in agreement with the literature, [29,30] which in conjunction with the preceding band gap energies yield corresponding conduction band edge potentials of −1.43 eV and −1.5 eV. The more negative conduction edge potential of the hierarchical Cu_2O nanocubes may accelerate charge transport during the photodegradation process. The oxidation state of Cu was also probed through Cu 2p core level XPS (Fig. 5b) revealing similar spectra for both nanocube types, with sharp photoemission features at 932.3 and 952.0 eV consistent with the $2p_{3/2}$ and $2p_{1/2}$ binding energies of either Cu_2O or Cu (which exhibit very similar chemical shifts). [31,32] The $2p_{3/2}$ spin-orbit component of the hierarchical nanocubes exhibited a slightly lower binding energy than their conventional counterpart, though whether due to initial or final state effects is unclear. Crucially, the 945.0 eV satellite characteristic of Cu^{2+} species was absent for both nanocubes, confirming phase purity [33].

Photoluminescence analysis was subsequently undertaken to examine photoexcited charge carrier lifetimes within the Cu_2O nanocubes. The emission spectra revealed a broad peak at 830 nm (Fig. 6), following 560 nm excitation, for both conventional and hierarchical nanocubes. However the integrated peak intensity of the latter is three times smaller, indicating that hierarchical Cu_2O nanocubes exhibit a far slower radiative recombination rate of photoexcited electron-hole pairs. Given the phase purity of conventional and hierarchical Cu_2O, and higher surface area:volume ratio of the latter, the slower radiative recombination is tentatively assigned to surface charge trapping of photoexcited charge carriers [34]. Textural properties determined by N_2 porosimetry (Fig. S2) highlight a very significant increase in the BET surface area of the hierarchical Cu_2O nanocubes ($21\ m^2\ g^{-1}$) compared with the conventional Cu_2O nanocube**s** ($4\ m^2\ g^{-1}$), which should dramatically increase the number of surface active sites available for photocatalytic processes. The five-fold increase in surface area is broadly comparable to the three-fold reduction in recombination, supporting increased charge trapping of photoexcited carriers in the hierarchical material. Since our synthetic protocol does not employ a mesostructured soft template [19], such as the Pluronic surfactants used for ordered mesoporous silicas [35] and alumina [36], neither our conventional nor hierarchical Cu_2O nanocubes are expected to exhibit well-defined mesoporosity. This is confirmed by the BJH pore size distributions shown in Fig. S2, which show that the conventional nanocubes are essentially non-porous, while the

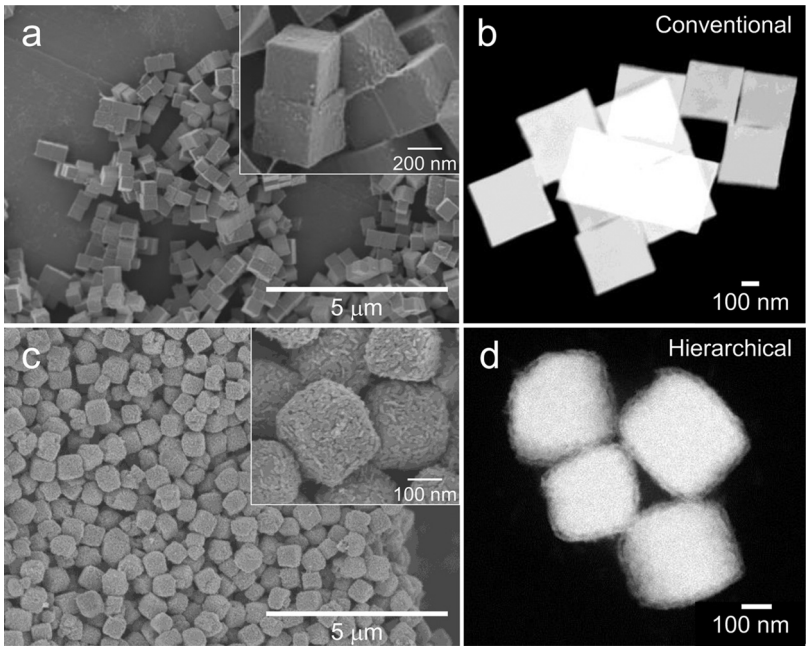

Fig. 2. (a,c) SEM and (b,c) dark field TEM images of conventional and hierarchical Cu_2O nanocubes. Insets show magnified images.

hierarchical nanocubes exhibit a broad range of mesopores spanning 1–6 nm and likely associated with interparticulate voids.

The photocatalytic efficacy of both types of Cu_2O nanocubes was explored for MB degradation as a prototypical organic pollutant [37]. Fig. 7a reveals the hierarchical Cu_2O nanocubes to be more active than conventional nanocubes towards MB photocatalytic degradation under visible light irradiation. Note that control experiments showed negligible MB photolysis over the same timescale in the absence of catalyst. Photodegradation over both Cu_2O nanocubes followed pseudo first-order kinetics as expected. [38] Surface area normalised rates of MB degradation (Fig. 7b) compensate for simple geometric differences between the hierarchical and conventional nanocubes, highlighting the former's superior intrinsic activity, which we ascribe to a combination of enhanced light absorption and charge transport properties (Figs. 4 and 6). Quantitative comparisons between different photocatalysts is hampered by the lack of standardization in photocatalytic activity testing, which is contingent on the number of incident/absorbed pho-

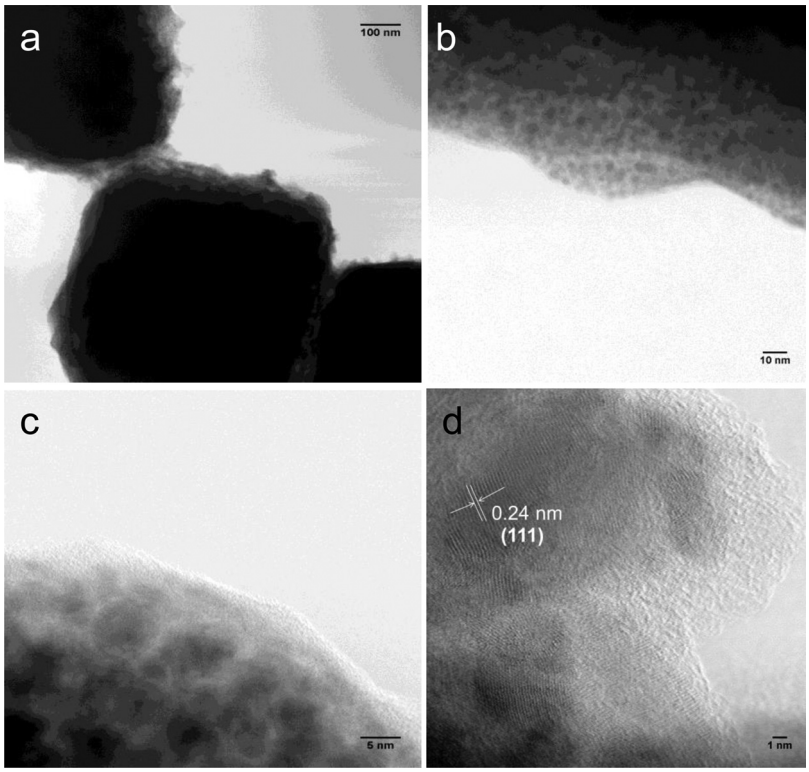

Fig. 3. TEM and HRTEM images of hierarchical Cu_2O nanocubes.

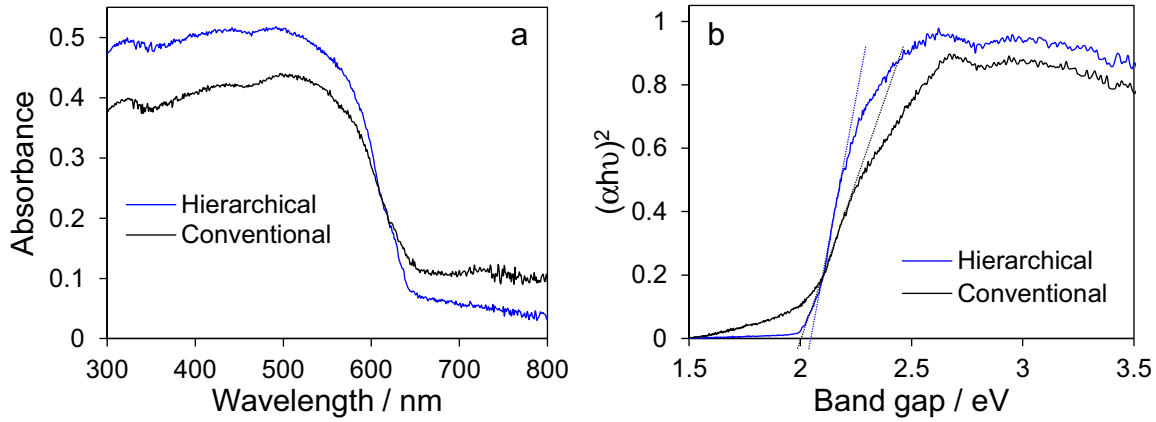

Fig. 4. (a) DRUVS absorption spectra, and (b) Tauc plot to determine optical band gaps of conventional and hierarchical Cu_2O nanocubes.

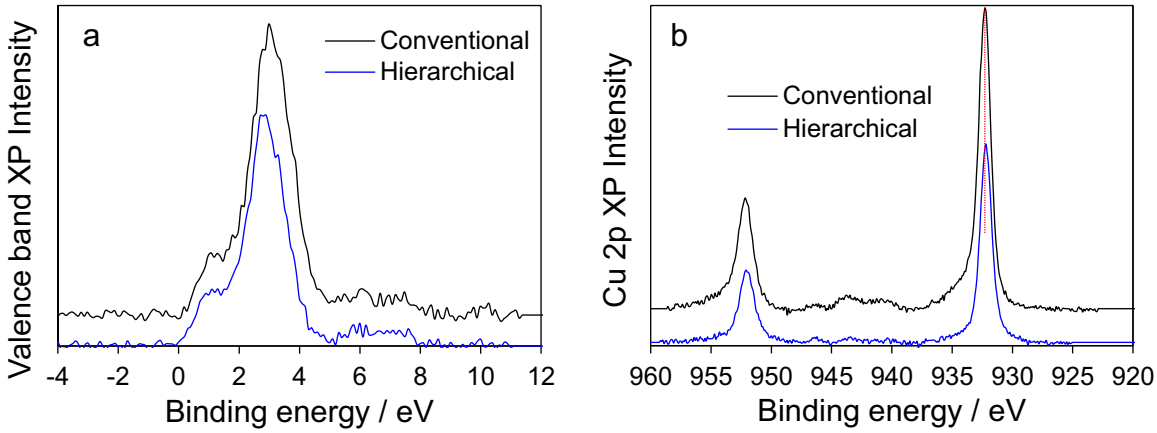

Fig. 5. (a) Valence band, and (b) Cu 2p XP spectra of conventional and hierarchical Cu_2O nanocubes. Spectra offset for clarity.

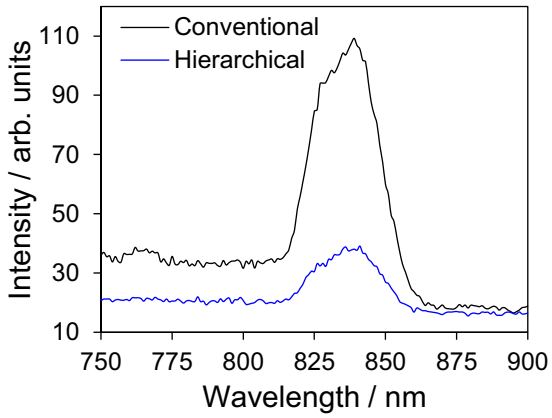

Fig. 6. Photoluminescence spectra of conventional and hierarchical Cu_2O nanocubes.

tons, and efficiency of their utilization in chemical conversion. Indeed the vast majority of photocatalytic studies do not report mass and surface area normalized rates. In large part this reflects the wide variance in light source (irradiance and spectral output) and photoreactor design (e.g. size and aspect ratio), which hinders quantification of the light flux impinging on catalysts. As a consequence, the photocatalytic activity for diverse reactions such as dye degradation and H_2 production, is often reported without reference to the number of incident photons or the surface area, despite the critical role of both. [3,39] Despite these complications, our hierarchical Cu_2O nanocubes perform exceptionally for MB degradation, with an initial rate of 0.6 compared to a rate of 0.008 $\mu mol.g^{-1}.min^{-1}$ for Cu_2O nanowires. [40]

The potential of hierarchical Cu_2O nanocubes for H_2 production from water splitting under visible light irradiation, was also investigated following the addition of 0.6 wt% Pt co-catalyst via wet-impregnation, and employing Na_2SO_3 as a sacrificial hole scavenger [8]. Fig. 8a shows that introduction of the hierarchy of self-assembled nanocrystals confers a striking increase in hydrogen productivity, which translates into a three-fold increase in the surface area normalised initial rate-enhancement (Fig. 8b). TEM of the platinized nanocubes (Fig. S3) show negligible differences in either Pt particle size or spatial distribution across the two nanocubes, and hence as with MB degradation, the different photoactivities must originate from different electronic/structural properties of the Cu_2O component. We therefore ascribe the superior intrinsic activity of the platinized hierarchical Cu_2O nanocubes for water splitting to a synergy between the higher energy charge carriers (arising from the slightly larger band gap), and improved visible light absorption and charge separation/transfer to active sites at the surface of Pt nanoparticles for reaction with water (evidenced by the slower charge recombination). As discussed above, quantitative comparisons of photocatalytic activity are hindered by a lack of standardization in the field. However, our rate of H_2 production and apparent quantum efficiency of 15 $\mu mol.g^{-1}.h^{-1}$ and 1.2% respectively, compare very favourably with representative literature values for 300–500 nm Cu_2O nanocrystals of 0.16 $\mu mol.g^{-1}.h^{-1}$ and 0.3%.[41]While higher rates of around 250 $\mu mol.g^{-1}.h^{-1}$ are reported for 1 wt% MoS_2 promoted 200–400 nm Cu_2O nanospheres

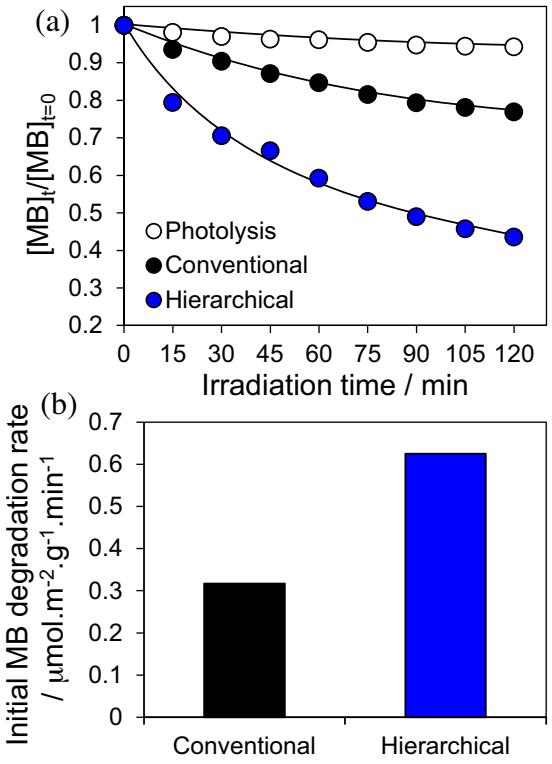

Fig. 7. (a) Visible light photocatalytic degradation of MB, and (b) normalised rates of MB degradation over conventional and hierarchical Cu_2O nanocubes.

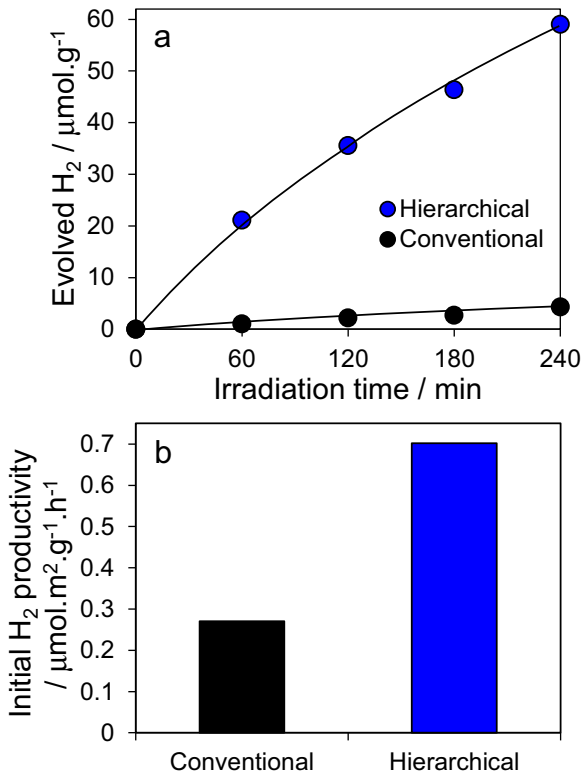

Fig. 8. (a) Visible light photocatalytic hydrogen production, and (b) normalised rates of hydrogen evolution over conventional and hierarchical Cu_2O nanocubes promoted with 0.6 wt% Pt co-catalyst.

[42] and 3 wt% Pt promoted Cu_2O-g-C_3N_4 nanocomposites, [29] these studies employed higher power light sources (350 W and 300 W respectively), and aqueous solutions of alcohols which were likely H-donors (25 vol% MeOH and 10 vol% triethanolamine respectively), while neither reported quantum efficiencies.

The excellent photocatalytic stability of our hierarchical Cu_2O nanocubes was evidenced through re-use experiments, which revealed retention of ≥90% of their initial surface area normalised rates of both methylene blue degradation and hydrogen production via water splitting (Fig. S4). Powder XRD further evidences the excellent stability of our hierarchical nanocubes, with the diffractograms of fresh and used catalysts unchanged (Fig. S5), confirming retention of the parent Cu_2O phase (and hence no photooxidation to CuO), and negligible nanocrystal sintering/dissolution. Mechanisms of dye photodegradation and solar H_2 production from water under visible light irradiation have been widely speculated, and we summarize the consensus in Fig. 9. Absorption of photons with energies equal to or exceeding the band gap of our Cu_2O nanocubes generates electron-hole pairs (Eq. (1)), with the resulting photoexcited electrons migrating to the conduction band (CB) with holes remaining in the valence band (VB). A fraction of the photogenerated charge carriers may undergo undesired direct recombination and associated fluorescence. Our photoluminescence spectra in Fig. 6 reveals that charge recombination is greatly suppressed in the hierarchical nanocubes relative to the conventional nanocubes, suggesting that photoinduced electron and hole migration to the surface of the hierarchical Cu_2O nanocubes (and their subsequent participation in redox catalysis) is much more efficient. For MB degradation, photoinduced holes in the VB readily react with hydroxyl ions (hole acceptors) to form hydroxyl radicals ($^{\bullet}OH$) (Eq. (2)), with corresponding photoexcited electrons in the CB reacting with dissolved O_2 to generate superoxide radicals $^{-\bullet}O_2$ (Eq. (3)). The resulting $^{-\bullet}O_2$ can further react with H_2O to increase the $^{\bullet}OH$ concentration (Eqs. (4)–(8)), with hydroxyl radicals responsible for MB oxidation. [43,44] Chithambararaj and co-workers have performed detailed mechanistic investigations into the photocatalytic bleaching of MB [45]. In addition to direct Cu_2O photoexcitation, dye degradation can also proceed via its sensitization of the semiconductor [46]. MB adsorbed at the surface of Cu_2O may undergo photoexcitation (absorption maximum ~670 nm), and resultant electron injection into the Cu_2O CB, facilitating charge separation. For H_2 evolution, electrons photoexcited into the Cu_2O CB are trapped by nanoparticles of the Pt co-catalyst, and subsequently react with H^+ from water to produce molecular H_2 (Eq. (9)). Simultaneously photogenerated holes in the VB are scavenged by SO_3^{2-} (Eq. (10)).

$$Cu_2O + h\nu \rightarrow Cu_2O^*(e^-_{CB} + h^+_{VB}) \quad (1)$$

$$h^+_{VB} + H_2O \rightarrow {}^{\bullet}OH + H^+ \quad (2)$$

$$O_2 + e^-_{CB} \rightarrow O_2^{\bullet -} \quad (3)$$

$$O_2^{\bullet -} + H^+ \rightarrow HO_2^{\bullet} \quad (4)$$

$$HO_2^{\bullet} + HO_2^{\bullet} \rightarrow H_2O_2 + O_2 \quad (5)$$

$$O_2^{\bullet -} + HO_2^{\bullet} \rightarrow O_2 + HO_2^- \quad (6)$$

$$HO_2^- + H^+ \rightarrow H_2O_2 \quad (7)$$

$$H_2O_2 + h\nu \xrightarrow{(Cu_2O)} 2\,{}^{\bullet}OH \quad (8)$$

$$2H_2O + 2e^-_{CB} \rightarrow H_2 + 2OH^- \quad (9)$$

$$SO_3^{-2} + 2h^+_{VB} + 2OH^- \rightarrow SO_4^{-2} + H_2O \quad (10)$$

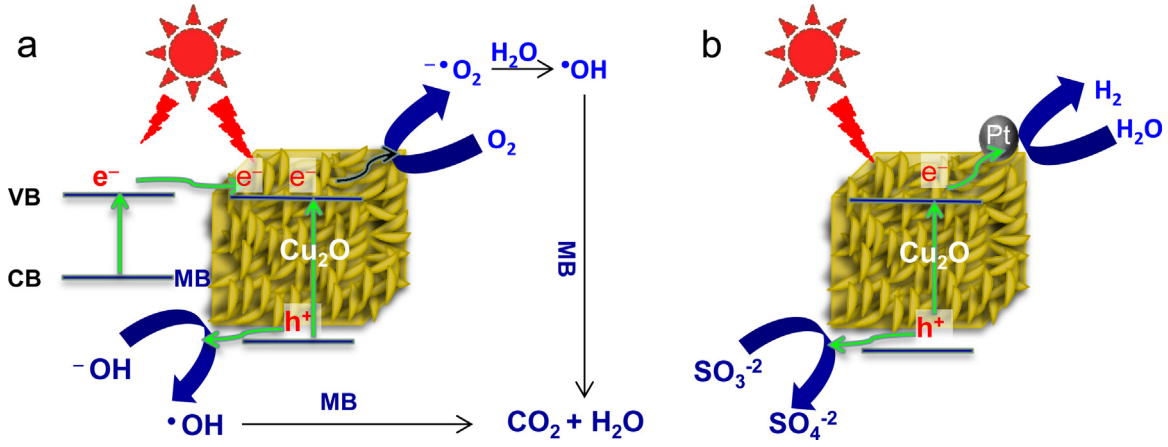

Fig. 9. Proposed mechanism of (a) photocatalytic MB degradation and (b) H_2 evolution under visible light irradiation over hierarchical Cu_2O nanocubes.

4. Conclusions

Phase-pure Cu_2O nanocubes with a hierarchical structure were successfully prepared by a one-pot synthesis employing PEG and glucose as a structure-directing agent and reductant respectively. This one-pot hydrothermal method avoids the use of hazardous reagents, e.g. hydrazine, [18,47] long reaction times, [42] or multiple steps e.g. hydrolysis and subsequent high temperature thermal processing. [41] Self-assembly of individual Cu_2O nanocrystals into hierarchical nanocubes increases their accessible surface active sites and optical/electronic properties compared to a conventional Cu_2O nanocube synthesis, conferring 100–200% rate-enhancements in the photocatalytic degradation of organic pollutants and hydrogen production from water splitting, and a good apparent quantum efficiency of 1.2%. Our simple methodology for the bottom-up assembly of ordered Cu_2O nanoarchitectures may be extendable to other semiconducting metal oxides, and additional photocatalytic reactions such as CO_2 photoreduction, and sensing applications.

Acknowledgements

We thank the EPSRC (EP/K021796/1 and EP/K029525/2) for financial support.

Appendix A. Supplementary data

Supplementary data associated with this article can be found, in the online version, at http://dx.doi.org/10.1016/j.apcatb.2016.02.038.

References

[1] M.N. Chong, B. Jin, C.W.K. Chow, C. Saint, Water Res. 44 (2010) 2997–3027.
[2] T. Hisatomi, J. Kubota, K. Domen, Chem. Soc. Rev. 43 (2014) 7520–7535.
[3] D. Chen, X. Zhang, A.F. Lee, J. Mater. Chem. A 3 (2015) 14487–14516.
[4] O.K. Dalrymple, E. Stefanakos, M.A. Trotz, D.Y. Goswami, Appl. Catal. B: Environ. 98 (2010) 27–38.
[5] A. Kubacka, M. Ferrer, M.L. Cerrada, C. Serrano, M. Sánchez-Chaves, M. Fernández-García, A. de Andrés, R.J.J. Riobóo, F. Fernández-Martín, M. Fernández-García, Appl. Catal. B: Environ. 89 (2009) 441–447.
[6] J. Ren, W. Wang, S. Sun, L. Zhang, L. Wang, J. Chang, Ind. Eng. Chem. Res. 50 (2011) 10366–10369.
[7] J. Kondo, Chem. Commun. (1998) 357–358.
[8] X. An, K. Li, J. Tang, ChemSusChem 7 (2014) 1086–1093.
[9] Z. Zheng, B. Huang, Z. Wang, M. Guo, X. Qin, X. Zhang, P. Wang, Y. Dai, J. Phys. Chem. C 113 (2009) 14448–14453.
[10] Y. Kwon, A. Soon, H. Han, H. Lee, J. Mater. Chem. A 3 (2015) 156–162.
[11] D. Wang, M. Mo, D. Yu, L. Xu, F. Li, Y. Qian, Cryst. Growth Des. 3 (2003) 717–720.
[12] L. Huang, F. Peng, H. Yu, H. Wang, Solid State Sci. 11 (2009) 129–138.
[13] L.-L. Ma, J.-L. Li, H.-Z. Sun, M.-Q. Qiu, J.-B. Wang, J.-Y. Chen, Y. Yu, Mater. Res. Bull. 45 (2010) 961–968.
[14] H. Yang, Z.-H. Liu, Cryst. Growth Des. 10 (2010) 2064–2067.
[15] Y. Zhang, B. Deng, T. Zhang, D. Gao, A.-W. Xu, J. Phys. Chem. C 114 (2010) 5073–5079.
[16] H. Zhou, J. Guo, P. Li, T. Fan, D. Zhang, J. Ye, Sci. Rep. (2013) 3.
[17] B. Naik, S.M. Kim, C.H. Jung, S.Y. Moon, S.H. Kim, J.Y. Park, Adv. Mater. Interfaces (2014) 1.
[18] Y. Zhao, W. Wang, Y. Li, Y. Zhang, Z. Yan, Z. Huo, Nanoscale 6 (2014) 195–198.
[19] C.M.A. Parlett, K. Wilson, A.F. Lee, Chem. Soc. Rev. 42 (2013) 3876–3893.
[20] Q. Zhao, D. Ju, X. Deng, J. Huang, B. Cao, X. Xu, Sci. Rep. (2015) 5.
[21] J. Du, X. Lai, N. Yang, J. Zhai, D. Kisailus, F. Su, D. Wang, L. Jiang, ACS Nano 5 (2010) 590–596.
[22] X. Wang, J.C. Yu, C. Ho, Y. Hou, X. Fu, Langmuir 21 (2005) 2552–2559.
[23] S. Sun, X. Zhang, X. Song, S. Liang, L. Wang, Z. Yang, Cryst. Eng. Commun. 14 (2012) 3545–3553.
[24] T.J. Hong, F.F. Tao, J.D. Lin, W. Ding, M.X. Lan, J. Solid State Chem. 228 (2015) 174–182.
[25] M. Deo, D. Shinde, A. Yengantiwar, J. Jog, B. Hannoyer, X. Sauvage, M. More, S. Ogale, J. Mater. Chem. 22 (2012) 17055–17062.
[26] L. Gou, C.J. Murphy, J. Mater. Chem. 14 (2004) 735–738.
[27] B.D. Viezbicke, S. Patel, B.E. Davis, D.P. Birnie, Phys. Status Solidi B 252 (2015) 1700–1710.
[28] K. Borgohain, N. Murase, S. Mahamuni, J. Appl. Phys. 92 (2002) 1292–1297.
[29] J. Chen, S. Shen, P. Guo, M. Wang, P. Wu, X. Wang, L. Guo, Appl. Catal. B: Environ. 152 (2014) 335–341.
[30] M.K. Hudait, M. Clavel, P. Goley, N. Jain, Y. Zhu, Sci. Rep. (2014) 4.
[31] J. Li, Z. Mei, L. Liu, H. Liang, A. Azarov, A. Kuznetsov, Y. Liu, A. Ji, Q. Meng, X. Du, Sci. Rep. (2014) 4.
[32] J. Espinos, J. Morales, A. Barranco, A. Caballero, J. Holgado, A. González-Elipe, J. Phys. Chemi. B 106 (2002) 6921–6929.
[33] J. Ghijsen, L. Tjeng, J. Van Elp, H. Eskes, J. Westerink, G. Sawatzky, M. Czyzyk, Phys. Rev. B 38 (1988) 11322.
[34] S. Kumar, B. Kumar, A. Baruah, V. Shanker, J. Phys. Chem. C 117 (2013) 26135–26143.
[35] C.M.A. Parlett, P. Keshwalla, S.G. Wainwright, D.W. Bruce, N.S. Hondow, K. Wilson, A.F. Lee, ACS Catal. 3 (2013) 2122–2129.
[36] C.M.A. Parlett, L.J. Durndell, K. Wilson, D.W. Bruce, N.S. Hondow, A.F. Lee, Catal. Commun. 44 (2014) 40–45.
[37] A. Mills, C. Hill, P.K. Robertson, J. Photochem. Photobio. A: Chem. 237 (2012) 7–23.
[38] B. Chai, X. Liao, F. Song, H. Zhou, Dalton Trans. 43 (2014) 982–989.
[39] K. Zhang, L. Guo, Catal. Sci. Technol. 3 (2013) 1672–1690.
[40] Y. Pan, S. Deng, L. Polavarapu, N. Gao, P. Yuan, C.H. Sow, Q.-H. Xu, Langmuir 28 (2012) 12304–12310.
[41] M. Hara, T. Kondo, M. Komoda, S. Ikeda, J.N. Kondo, K. Domen, M. Hara, K. Shinohara, A. Tanaka, Chem. Commun. (1998) 357–358.
[42] Y.-F. Zhao, Z.-Y. Yang, Y.-X. Zhang, L. Jing, X. Guo, Z. Ke, P. Hu, G. Wang, Y.-M. Yan, K.-N. Sun, J. Phys. Chem. C 118 (2014) 14238–14245.
[43] M. Stylidi, D.I. Kondarides, X.E. Verykios, Appl. Catal. B: Environ. 47 (2004) 189–201.
[44] Z. Chen, D. Li, W. Zhang, Y. Shao, T. Chen, M. Sun, X. Fu, J. Phys. Chem. C 113 (2009) 4433–4440.
[45] A. Chithambararaj, N.S. Sanjini, A.C. Bose, S. Velmathi, Catal. Sci. Technol. 3 (2013) 1405–1414.
[46] S. Tonda, S. Kumar, S. Kandula, V. Shanker, J. Mater. Chem. A 2 (2014) 6772–6780.
[47] F. Meng, S. Jin, Nano Lett. 12 (2012) 234–239.